Front. Earth Sci. 2023, 17(2): 589–603
https://doi.org/10.1007/s11707-022-0997-y

RESEARCH ARTICLE

Simulating CO_2 profiles using NIES TM and comparison with HIAPER Pole-to-Pole Observations

Ci SONG[1], Shamil MAKSYUTOV[2], Jiong SHU (✉)[3]

1 College of Science, Zhongyuan University of Technology, Zhengzhou 450007, China
2 National Institute for Environmental Studies, Tsukuba 305-8506, Japan
3 Key Laboratory of Geographic Information Science, Institute of Climate Change, East China Normal University, Shanghai 200241, China

Abstract We present a study on validation of the National Institute for Environmental Studies Transport Model (NIES TM) by comparing to observed vertical profiles of atmospheric CO_2. The model uses a hybrid sigma-isentropic (σ–θ) vertical coordinate that employs both terrain-following and isentropic parts switched smoothly in the stratosphere. The model transport is driven by reanalyzed meteorological fields and designed to simulate seasonal and diurnal cycles, synoptic variations, and spatial distributions of atmospheric chemical constituents in the troposphere. The model simulations were run for combination of biosphere, fossil fuel, air-ocean exchange, biomass burning and inverse correction fluxes of carbon dioxide (CO_2) by GOSAT Level 4 product. We compared the NIES TM simulated fluxes with data from the HIAPER Pole-to-Pole Observations (HIPPO) Merged 10-s Meteorology, Atmospheric Chemistry, and Aerosol Data, including HIPPO-1, HIPPO-2 and HIPPO-3 from 128.0°E to 84.0°W, and 87.0°N to 67.2°S. The simulation results were compared with CO_2 observations made in January and November, 2009, and March and April, 2010. The analysis attests that the model is sufficient to simulate vertical profiles with errors within 1–2 ppmv, except for the lower stratosphere in the northern hemisphere high latitudes.

Keywords HIPPO, CO_2, simulation, vertical profile, NIES-TM

1 Introduction

Atmospheric carbon dioxide (CO_2) is a primary radiative forcing greenhouse gas produced by human activities. It causes the most global warming (IPCC, 2016), and its atmospheric concentration has been increasing at a progressively faster rate each decade because of rising global emissions (Raupach et al., 2007). The monitoring of CO_2 from space is intended to identify the sources and sinks of greenhouse gases generated by human and natural activities. A number of satellites are actively monitoring greenhouse gases (e.g., GOSAT, SCIAMACHY, AIRS, IASI) to answer this question, and retrieval algorithms for CO_2 have been developed for these satellite observation data to provide more accurate estimates of CO_2 concentrations using several different methods.

The sparseness and spatial inhomogeneity of existing surface network have limited our ability to understand the quantity and spatiotemporal distribution of CO_2 sources and sinks (Scholes et al., 2009). Recent studies of global sources and sinks of greenhouse gases, and their concentrations and distributions, have been mainly based on *in situ* surface measurements (GLOBALVIEW-CO_2, 2013). The diurnal and seasonal "rectifier effect" , the covariance between surface fluxes and the strength of vertical mixing, and the proximity of local sources and sinks to surface measurement sites all have an influence on the measured and simulated concentrations, and complicate the interpretation of results (Denning et al., 1996; Gurney et al., 2004; Baker et al., 2006). Comparatively speaking, the vertical integration of mixing ratio divided by surface pressure, denoted as the column-averaged dry-air mole fraction (DMF; denoted XG for gas G) is much less sensitive to the vertical redistribution of the tracer within the atmospheric column (e.g., due to variations in planetary boundary layer (PBL) height), and it is more easily related to the underpinning surface fluxes than near surface concentrations (Yang et al., 2007). Thus, column-averaged measurements and simulations are expected to be very useful for improving our understanding of carbon cycle (Yang et al., 2007; Keppel-Aleks et al., 2010; Wunch et al., 2011; Parker et al., 2011). In addition, atmospheric transport

Received February 13, 2022; accepted June 23, 2022

E-mail: jshu1952@126.com, jshu@geo.ecnu.edu.cn

has to be accounted for when analyzing the relationships between observations of atmospheric constituents and their sources/sinks near the earth's surface or through the chemical transformation in the atmosphere. As a result, reliable estimates of climate change depend upon our ability to predict atmospheric CO_2 concentrations, which requires further investigation of the CO_2 sources, sinks, and atmospheric transport.

Global atmospheric tracer transport models are usually applied to studies of the global cycles of long-lived atmospheric trace gases, such as CO_2 and methane (CH_4), because the long-lived atmospheric tracers exhibit observable global patterns (e.g., the interhemispheric gradient of the concentration). Global three-dimensional chemistry transport models (hereafter referred to as CTMs), driven by actual meteorology from numerical weather predictions, and global circulation models (GCMs) play a crucial role in assessing and predicting change in the composition of the atmosphere due to anthropogenic activities and natural processes (Rasch et al., 1995; Jacob et al., 1997; Denning et al., 1999; Bregman et al., 2006; Law et al., 2008; Maksyutov et al., 2008, 2021; Patra et al., 2008).

The transport modeling is done on different scales ranging from local plume spread, regional mesoscale transport to global scale analysis, depending on the scale of the phenomena that are studied. Forward modeling is used to estimate tracer concentrations in regions that lack observation data and to identify the features of tracer transport and dispersion (Law et al., 2008; Patra et al., 2008). Inverse methods are generally applied when interpreting the data, and atmospheric transport models provide the link between surface gas fluxes and their subsequent influence on atmospheric concentrations (Rayner and O'Brien, 2001; Patra et al., 2003a, 2003b; Gurney et al., 2004; Baker et al., 2006). Global modeling analysis helps to identify the relative contribution of land and oceans in the northern and southern hemispheres to the interhemispheric concentration differences of CO_2, CH_4, carbon monoxide (CO) and other tracer species (Bolin and Keeling, 1963; Hein et al., 1997). For stable and slowly reacting chemical species, a number of studies have derived information on the spatial and temporal distribution of surface sources and sinks by applying transport models and atmospheric observations (Tans et al., 1990; Rayner et al., 1999).

There are several factors that strongly influence model performance: the numerical transport algorithm used, meteorological data, grid type and resolution. In tracer transport calculations, semi-Lagrangian transport algorithms are often used in combination with finite-volume models. In these algorithms, the losses of total tracer mass are possible. While such losses are often negligible for short-term transport simulations, they can seriously distort the global trends and tracer budgets in long-term simulations. To avoid such losses, various mass-fixing schemes have been applied (Hack et al., 1993; Rasch et al., 1995). Although the use of mass fixers can prevent mass losses, there remains a possibility of predicting distorted tracer concentrations. By contrast, when using a flux-form transport algorithm, the total tracer mass is conserved and thus the issue of mass losses can be eliminated, provided that the flow is conserved. The use of numerical schemes with limiters leads to distorted tracer concentrations and affects the linearity. Thus, to accurately calculate the tracer concentration in a forward simulation and to use the model in inverse modeling, we employed a flux-form version of global off-line, three-dimensional chemical NIES TM.

The synoptic and seasonal variability in XCO_2 is driven mainly by changes in surface pressure, tropospheric volume-mixing ratio (VRM) and stratospheric concentration, which is affected in turn by changes in tropopause height. The effects of variations in tropopause height are more pronounced with increasing contrast between stratospheric concentrations. Many CTMs demonstrate some common failings of model transport in the stratosphere (Hall et al., 1999). The difficulty of accurately representing dynamical processes in the upper troposphere (UT) and lower stratosphere (LS) has been highlighted in recent studies (Mahowald et al., 2002; Waugh and Hall, 2002; Monge-Sanz et al., 2007). While there are many contributing factors, the principal factors affecting model performance in vertical transport are meteorological data and vertical grid layout (Monge-Sanz et al., 2007).

The use of different meteorological fields in driving chemical transport models can lead to diverse distribution of chemical species in the UTLS region (Douglass et al., 1999). The quality of wind data provided by numerical weather predictions is another crucial factor for tracer transport (Jöckel et al., 2001; Stohl et al., 2004; Bregman et al., 2006). Wind fields produced by the Data Assimilation System (DAS) are commonly used for driving CTMs. Spurious variability, or "noise", introduced via the assimilation procedure affects the quality of meteorological data through a lack of suitable observations or inaccurate treatment of model biases (Bregman et al., 2006). This negative effect is proportional to the dynamic time scale and increases with operational time (Maksyutov et al., 2008). The most sensitive area in this regard is the lower stratosphere in tropical regions, where large volumes of air move upward from the troposphere to the stratosphere. A lack of observations makes this region the most challenging in terms of data assimilation. Bregman et al. (2006) pointed out that the additional difficulty of detecting model biases is caused by the fact that the tropical atmosphere is not in geostrophic equilibrium. Schoeberl et al. (2003) suggested that GEOS DAS (Geodetic Earth Orbiting Satellite Data Assimilation System) is less suitable for long-term stratospheric transport studies than wind from a general circulation model. At the same time, improvements to DAS itself (ECMWF ERA-Interim reanalysis; Dee and Uppala, 2009)

and the development of special products for transport models (MERRA: Modern Era Retrospective-analysis for Research and Applications; Bosilovich et al., 2008) help to improve the accuracy of atmospheric circulation when using off-line models (Monge-Sanz et al., 2007).

Belikov et al. (2013) evaluated the simulated XCO_2 column-averaged DMF against daily ground-based high-resolution Fourier Transform Spectrometer (FTS) observations measured at 12 sites of the Total Column Observing Network (TCCON), which provides an essential validation resource for the Orbiting Carbon Observatory (OCO), SCIAMACHY, and GOSAT. This paper presents the application of the standard isentropic transport model with HIAPER Pole-to-Pole Observations (HIPPO) Merged 10-s Meteorology, Atmospheric Chemistry, and Aerosol Data. These data have high time resolution because of the underlying 1-s in situ frequency measurement, and vertical resolution, because of the GV flight plan performed 787 vertical ascents/descents from the ocean/ice surface up to the tropopause (Wofsy et al., 2012). In addition, this paper provides the detailed description of model information, meteorology data set and HIPPO data, and a validation of CO_2 vertical profiles comparing against the HIPPO observations, followed by a discussion and conclusions.

2 Model features and operation

In this section, we describe the features and the use of NIES TM (denoted NIES-08, li). As Belikov et al. (2011, 2013, 2019) described, the latest improved version of NIES TM model uses the (θ–σ) hybrid sigma-isentropic vertical coordinate that is isentropic in the UTLS region but terrain-following in the free troposphere. This designed coordinate helps to simulate vertical motion in the isentropic part of grid above level 350 K. Basic physical model features include the flux-form dynamical core with a third-order van Leer advection scheme, a reduced latitude-longitude grid, a horizontal flux-correction method for mass balance, and turbulence parameterization.

2.1 Meteorological data used in the simulation

NIES TM is an off-line model driven by Japanese reanalysis data, covering more than 30 years from 1 January 1979 to present (Onogi et al., 2007). The Japanese 25-year Reanalysis (JRA-25) used by Belikov et al. (2013) covers the period from1979 to 2004, and is the product of Japan Meteorological Agency (JMA) and Central Research Institute of Electric Power Industry (CRIEPI). After 2005, near real-time operational analysis using the same assimilation system as JRA-25 continues to be carried out as JMA Climate Data Assimilation System (JCDAS). The JRA-25/JCDAS data set is distributed on a Gaussian horizontal grid T106 (320 × 160) with 40 hybrid σ–p levels. The 6-hourly time step of JRA-25/JCDAS is coarser than the 3-hourly data from the National Centers for Environmental Prediction (NCEP) Global Forecast System (GFS) and Global Point Value (GPV) data sets, which were used in previous model versions (Belikov et al., 2011). However, with better vertical resolution (40 levels on a hybrid σ–p grid versus 25 and 21 pressure levels for GFS and GPV, respectively), a vertical grid with 32 levels can be realized (versus the 25 levels previously used), so as to obtain more detailed boundary layer and UTLS region resolution (Table 1).

Used to calculate vertical transport in the θ-coordinate domain of hybrid sigma-isentropic coordinate, the 2-D monthly distribution of climatological heating rate is prepared from JCDAS reanalysis data, which are provided as the sum of short- and long-wave components at pressure levels.

Table 1 Vertical grid levels of the NIES TM model

	H/km	$\sigma=P/P_s$	≈△/m	ξ (σ-θ grid levels)/K	Number of levels
Near surface layer	0–2	10–0795	250	–	8
Free troposphere	2–12	0795–0195	1000	–,330,350,	10
			1000	365,380,400,415,	
				435,455,475,500,	
Upper troposphere and stratosphere	12–40	0195–0003	2000	545,	14
			–	590,665,850,	
				1325,1710	
				Total levels:	32

Notes: H, height; P, atmospheric pressure; P_s, surface atmospheric pressure; △, vertical integral step; ξ, the level of the sigma-isentropic grid.

2.2 HIPER Pole-to-Pole data

The HIPPO study investigated the carbon cycle and greenhouse gases at various heights (from 0 to 16 km) in the western hemisphere through annual cycle. HIPPO is supported by the National Science Foundation (NSF) and its operations are managed by the Earth Observing Laboratory (EOL) of the National Center for Atmospheric Research (NCAR). Its base of operations is the EOL Research Aviation Facility (RAF) at the Rocky Mountain Metropolitan Airport (RMMA) in Jefferson County, Colorado. The main goal of HIPPO was to determine the global distribution of CO_2 and other trace atmospheric gases by sampling at several heights and latitudes (from 0 to 16 km, 87.0°N to 67.2°S) in the Pacific Basin.

The data set used in this paper includes the merged 10-s data product of meteorological, atmospheric chemistry, and aerosol measurements from three HIPPO Missions 1 to 3. The three missions took place from January, 2009 to April, 2010; HIPPO-1 (20090109–20090126), HIPPO-2 (20091102–20091122), and HIPPO-3 (20100324–20100415), ranging from 128.0°E to 84.0°W, and 87.0°N to 67.2°S

(Table 2). All data are provided in a single space-delimited format ASCII file (available at EOL website).

HIPPO measured atmospheric constituents along transects running approximately pole-to-pole over the Pacific Ocean and recorded hundreds of vertical profiles from the ocean/ice surface up to the tropopause five times during four seasons from January, 2009 to September, 2011. HIPPO provides the first high-resolution vertically resolved global survey, which investigates a comprehensive suite of atmospheric trace gases and aerosols pertinent to understanding carbon cycle and challenging global climate models. The 10-s merge product applied in this study was derived by combining the navigation and atmospheric structure parameters of the National Science Foundation (NSF)/NCAR GV aircraft, including position, time, temperature, pressure, and wind speed reported at 1-s frequency, as well as meteorological, atmospheric chemistry and aerosol measurements conducted by several teams of investigators on a common time and position basis.

Table 2 Temporal and spatial (horizontal) coverage of HIPPO mission flights

Missions sampling	Dates	Vertical profiles flown	Flight path notes
HIPPO-1	January 8–30, 2009	138	Northern polar flight #1 reached 80°N, Southern ocean flight reached 67°S, 175°W (no return to the Arctic a second time)
HIPPO-2	October 31 to November 22, 2009	148	Northern polar flight #1 reached 80°N, Southern ocean flight reached 66°S, and 174°W, Northern polar flight #2 reached 83°N
HIPPO-3	March 24 to April 16, 2010	136	Northern polar flight #1 reached 84.75°N, Southern ocean flight reached 66.8°S, 170°E, Northern polar flight #2 reached 85°N

2.3 Model setup

The standard model was run with three HIPPO missions to study atmospheric tracer transport and the ability of the model to reproduce column-averaged DMF and atmospheric CO_2 vertical profile. The model was run at a horizontal resolution of 2.5° × 2.5° and 32 vertical levels from surface to 3 hPa.

The CO_2 simulations started on January 1, 2009, November 1, 2009 and March 1, 2010 for three HIPPO missions 1 to 3, respectively, with individual initial 3D tracer distributions using the global prior fluxes of biosphere-atmosphere and air-ocean exchange, fossil fuel emissions, biomass burning, and GOSAT Level 4A inverse model correction (Maksyutov et al., 2013, 2021). These fluxes are provided by climate average of global monthly CO_2 fluxes estimated by GLOBALVIEW and GOSAT SWIR Level 2 XCO_2 data. As we use same set of fluxes and same version of transport model as GOSAT Level 4 product, the flux corrections provided by GOSAT Level 4 product provide optimal fit for available observations.

3 Discussion

The current model versions have been used in several tracer transport studies and were evaluated through participation in transport model intercomparisons (Niwa et al., 2011; Patra et al., 2011). The simulation results of the tracer transport model show consistency with observations in the near surface layer and in the free troposphere. However, the model performance in the UTLS region has not been evaluated in detail against other observations.

3.1 Comparison with CO_2 observations

Figure 1 shows the scatters diagram of modeled results versus total column of HIPPO-1, 2, 3. The majority of points are within 95% confidence interval of total CO_2 column concentration. Modeled HIPPO-1's precision successively exceeds 2 and 3, inferring the simulation results with the relevant either seasonal changes or data quality.

The simulation results of CO_2 concentration time-varying for HIPPO-1 using the standard model display good performance and weak dispersion of concentrations. The validation results (Fig. 2(a)) show that approximately 69.2% of absolute biases are within 1 ppmv, approximately 92.3% are within 2 ppmv, and only 7.7% exceed 3 ppmv. Furthermore, as shown by root-mean-square error (RMSE) with time, during most days in January, the model values' dispersion was small compared with observed values, apart from the first few days of the month. According to the simulation results of HIPPO-1 observed and simulated latitude-varying CO_2 concentration data, the comparison values always underestimate the atmospheric XCO_2, and the differences are all within 1.5 ppmv in the southern hemisphere, and vice versa in the northern hemisphere with 85.8% of differences under 1.1 ppmv. Figure 2(b) shows that the larger biases usually occur in the northern hemisphere high latitudes. The RMSE also reflects the instability of simulated values in

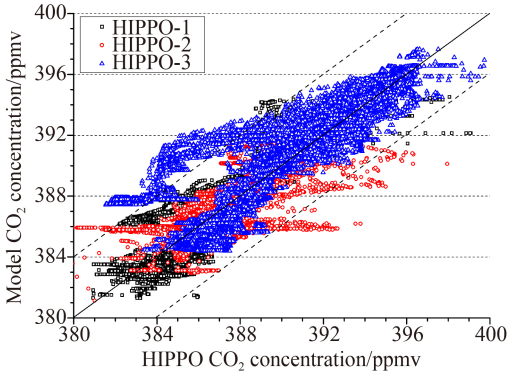

Fig. 1 Scatter diagram of modeled and observed CO_2 of HIPPO-1 (black square), 2 (red circle), 3 (blue triangle). Dotted lines show a 95% confidence interval of CO_2 concentration.

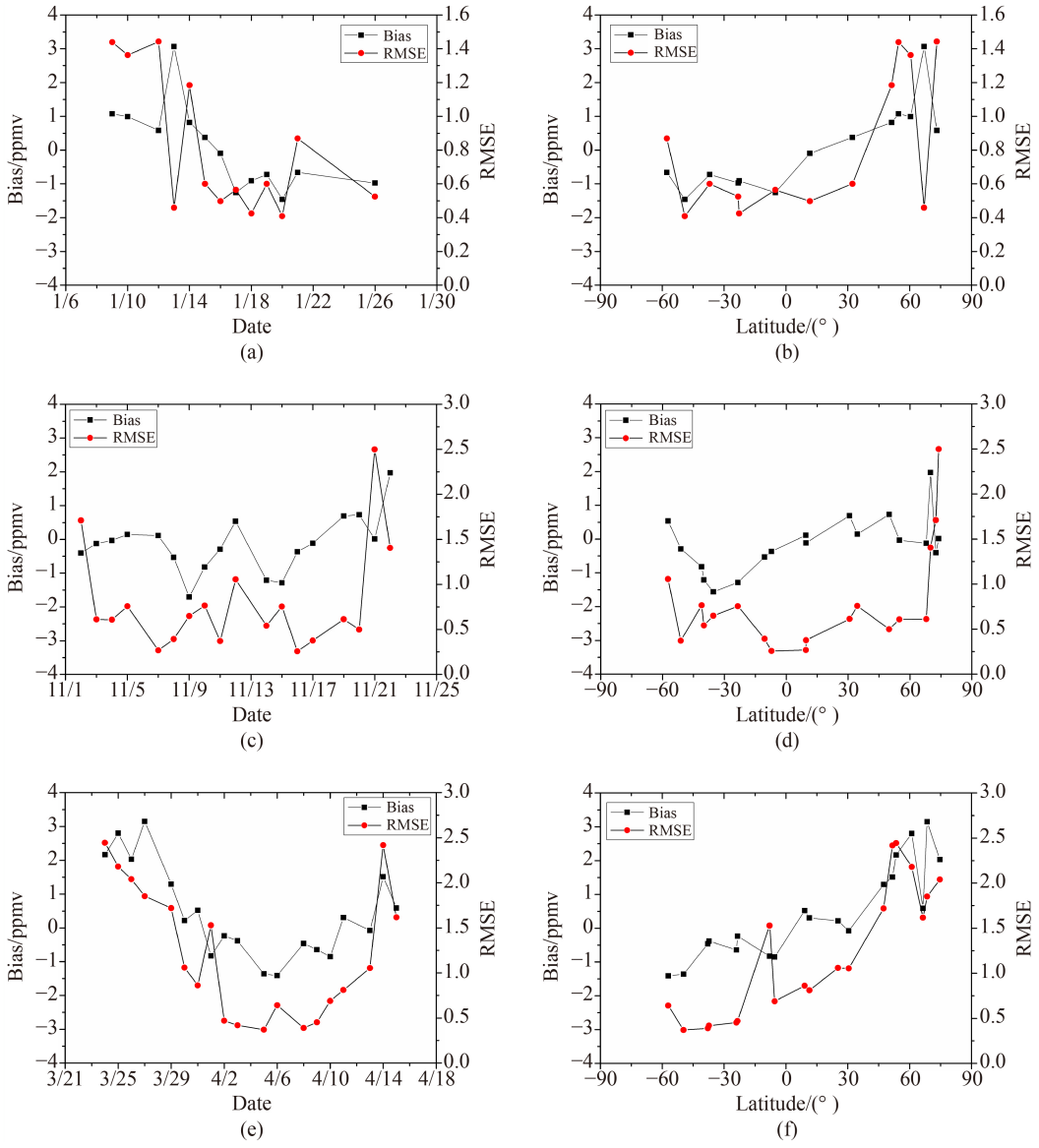

Fig. 2 Bias (simulation-observation, black square) and RMSE (red circle) of time- ((a) HIPPO-1, (c) HIPPO-2, (e) HIPPO-3) and latitude-varying ((b) HIPPO-1, (d) HIPPO-2, (f) HIPPO-3) CO_2 concentration data.

the northern hemisphere high latitudes.

For HIPPO-2 data from November 2 to 22, 2009, the absolute biases of observed and simulated time-varying are all within 2 ppmv, and 77.8% of differences are less than 1 ppmv (Fig. 2(c)). Approximately 5/6 of the data over this month show relative stability. Similarly with HIPPO-1, the simulation results are always underestimates in the southern hemisphere and overestimates in the northern hemisphere. As shown in Fig. 2(d), the complete simulation displays good performance, apart from one day in the northern hemisphere high latitudes. Similarly, RMSE shows good stability in the southern hemisphere, especially in the middle and low latitudes of the southern hemisphere. The model also simulates well in the northern hemisphere, especially from 45°N to 70°N.

Based on HIPPO-3 data from March 24 to April 15, 2010, the model simulation overestimates in March and underestimates in April. As shown in Fig. 2(e), in March, the biases over several days were over 2 ppmv, and one of these days exceeded 3 ppmv. However, absolute biases were all within 2 ppmv in April, and 75% of absolute biases were less than 1 ppmv, which suggests relatively good performance by the model simulation. As shown by RMSE, the data for the last days in March were disperse. However, 81.8% of the data in April showed comparatively good stability. The absolute biases are all under 1.5 ppmv in the southern hemisphere, and are also within 2 ppmv for the middle and low latitudes of the northern hemisphere (Fig. 2(f)). However, a relatively large difference occurs at the northern hemisphere high latitudes, at one point exceeding 3 ppmv. Furthermore, RMSE become

greater with latitude from the southern to northern hemisphere, inferring the simulation results are increasingly disperse with increasing latitude.

3.2 Validation of CO_2 vertical profiles

The GV flight plan performed 787 vertical ascents/descents from the ocean/ice surface/land surface to the tropopause. Two maximum height ascents were planned per flight to the tropopause/LS; one in the first half and the other in the second half of research flight. In between, several vertical profiles from below the PBL to the middle troposphere (1000–28000 feet) were flown. Profiles were flown approximately every 2.2° of latitude with 4.4° between consecutive near surface or high height samples. Rate of climb and descent was 1500 ft/minute (457 m/minute). During these profiles, the GV averaged a ground speed of approximately 175 m/second, or 10 km/minute.

Most of a flight was conducted below the international Reduced Vertical Separation Minimum (RVSM), usually 29000 ft or 8850 m, to allow the GV to descend and climb constantly to collect data at different heights throughout the troposphere. All flight plans were subject to modifications depending on local atmospheric conditions and approval by air traffic control. Most profiles extended from approximately 300 to 8500 m height, constrained by air traffic, but significant profiling extended above approximately 14 km.

One of the aims of this paper was to validate the model column-averaged concentration against the typical HIPPO flight plans, and we checked the variability of CO_2 concentrations from Mission 1 to 3 by HIPPO merged 10-s meteorology, atmospheric chemistry, and aerosol measurements. For each mission, several hundred vertical profiles were produced. We have only selected the vertical profiles from near surface to LS to compare the simulations using the standard model with observations. Each mission can be divided into six parts for analysis; the low, middle and high latitudes in the southern and northern hemispheres, respectively.

Figure 3 presents us the change of flight height and bias by subtracting observation by simulation of HIPPO-1, 2, 3 with latitude. The number of observations number in these three missions is 17621, 23451 and 22372, respectively. A large number of observations provide a basis for model validation. According to the variation of flight height with latitude in Fig. 3, we only select the CO_2 profiles from the near surface to the lower stratosphere. According to the above rule, 24, 34, and 35 profiles are selected for HIPPO-1, 2, 3 respectively. Then, because the profile shapes of each latitude zone are similar, we select a profile of low, middle and high latitude in the Northern and Southern hemisphere from the selected profiles of each mission. Seen from Fig. 3, relatively large biases occur repeatedly in the high latitude of the Northern Hemisphere.

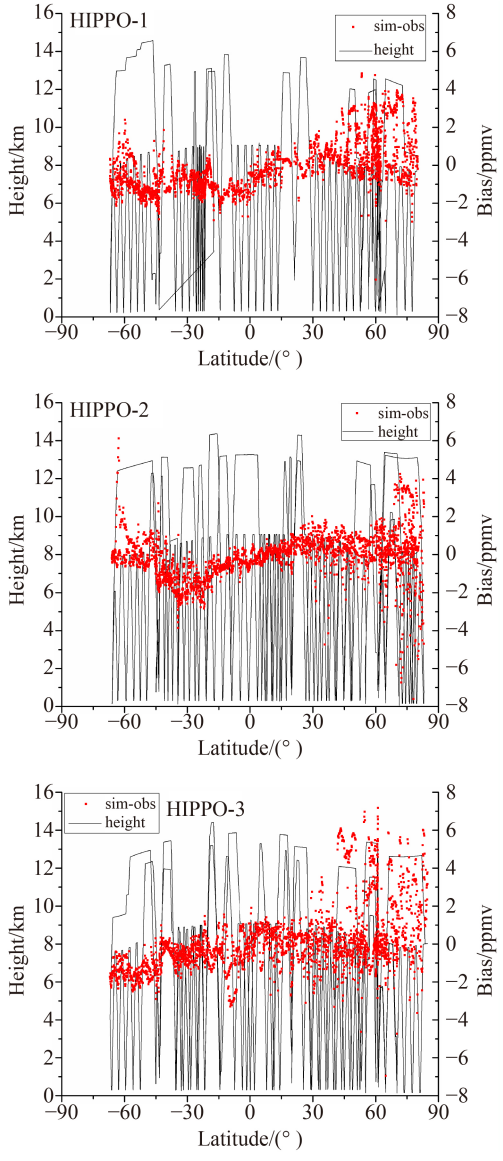

Fig. 3 Change of flight height and difference between simulation and observation of HIPPO-1, 2, 3 with latitude.

For HIPPO-1, the simulated value in the southern hemisphere is always less than the observation value and vice versa in the northern hemisphere. The deviation of the whole contour from the near surface to LS is less than 2 ppmv. However, it increases from 2 to 4 ppmv above 10 km covering the northern hemisphere high latitudes.

Figure 4 shows the comparison of simulation results and observations for data from the near surface to LS in low, middle and high latitude. In low latitudes, as shown in Figs. 4(c) and 4(d), the simulation performed very well compared with observations. All deviations are within 1 ppmv, except for the deviation of about 2 ppmv in the tropopause in Fig. 4(d). In the middle and high latitudes, the two hemispheres are different. In the southern hemisphere, expect for the LS area in Fig. 4(a) and 2–6 km area in Fig. 4(b), most deviations are within 2 ppmv. In

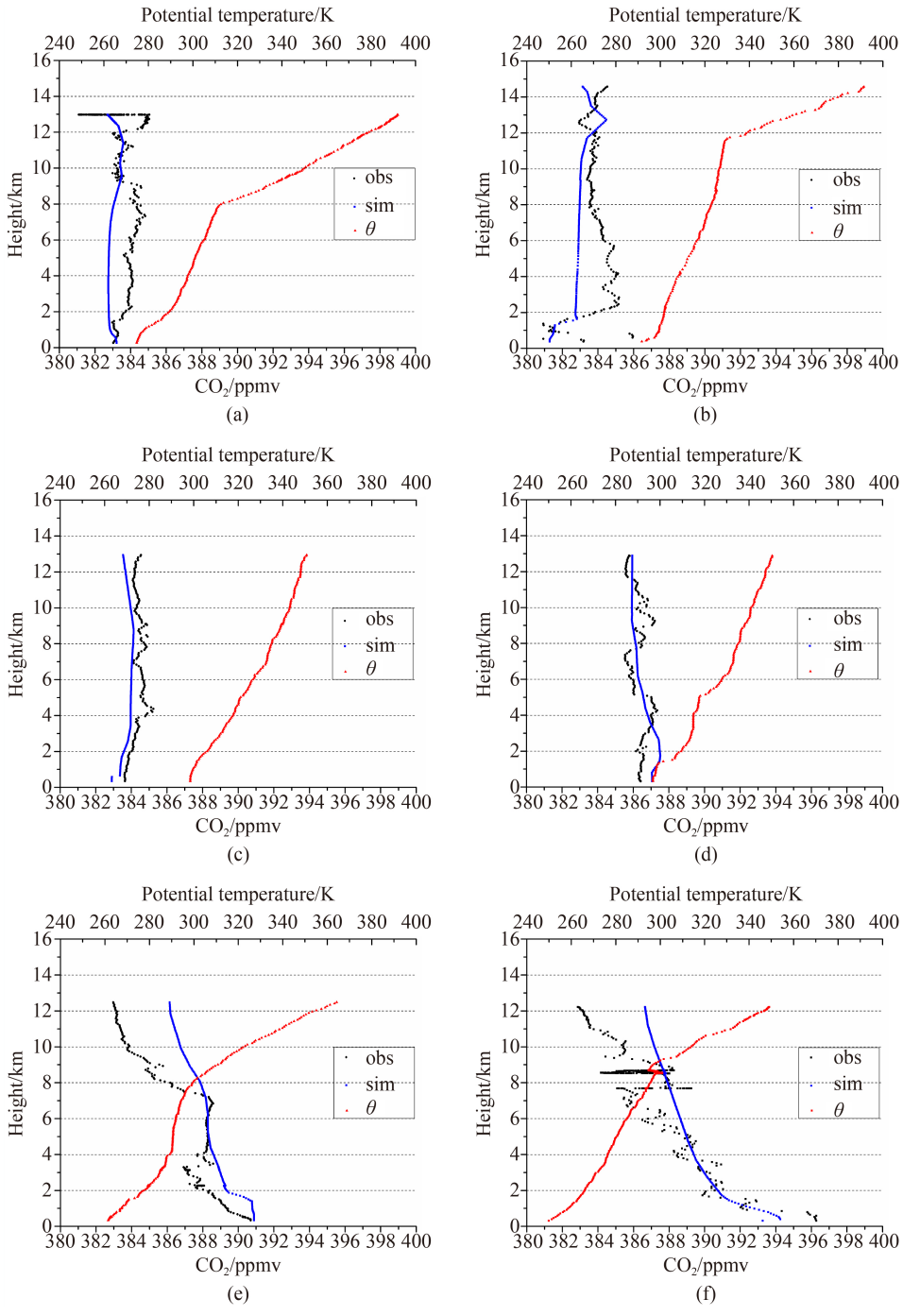

Fig. 4 Vertical profiles from near surface to the LS for HIPPO-1, Figures represent the vertical profiles of observation (black square), simulation (blue square) and potential temperature (red square) in Southern ((a) high, (b) middle, (c) low latitude), and Northern Hemisphere ((d) low, (e) middle, (f) high latitude).

the northern hemisphere (Figs. 4(e) and 4(f)), apart from UTLS, the simulated vertical profiles show good performances with a deviation of less than 2 ppmv. Some large biases occurred in the UTLS exceeding 4 ppmv when potential temperature gradient increased rapidly with height. For details, Fig. 5 presents us the biases of simulation minus observation corresponding to Figs. 4(a)–4(f), respectively.

HIPPO-2 data and HIPPO-1 data are generally similar in positive and negative bias distribution. However, anomalies occurred at approximately 60°S and 75°N latitudes, showing positive and negative biases, respectively, with some biases exceeding 6 ppmv. Figure 6(a) is the vertical profile of the southern hemisphere at high latitudes, which clearly shows that the simulation matches well with observations from the near surface to the tropopause. However, large biases occur above 8 km.

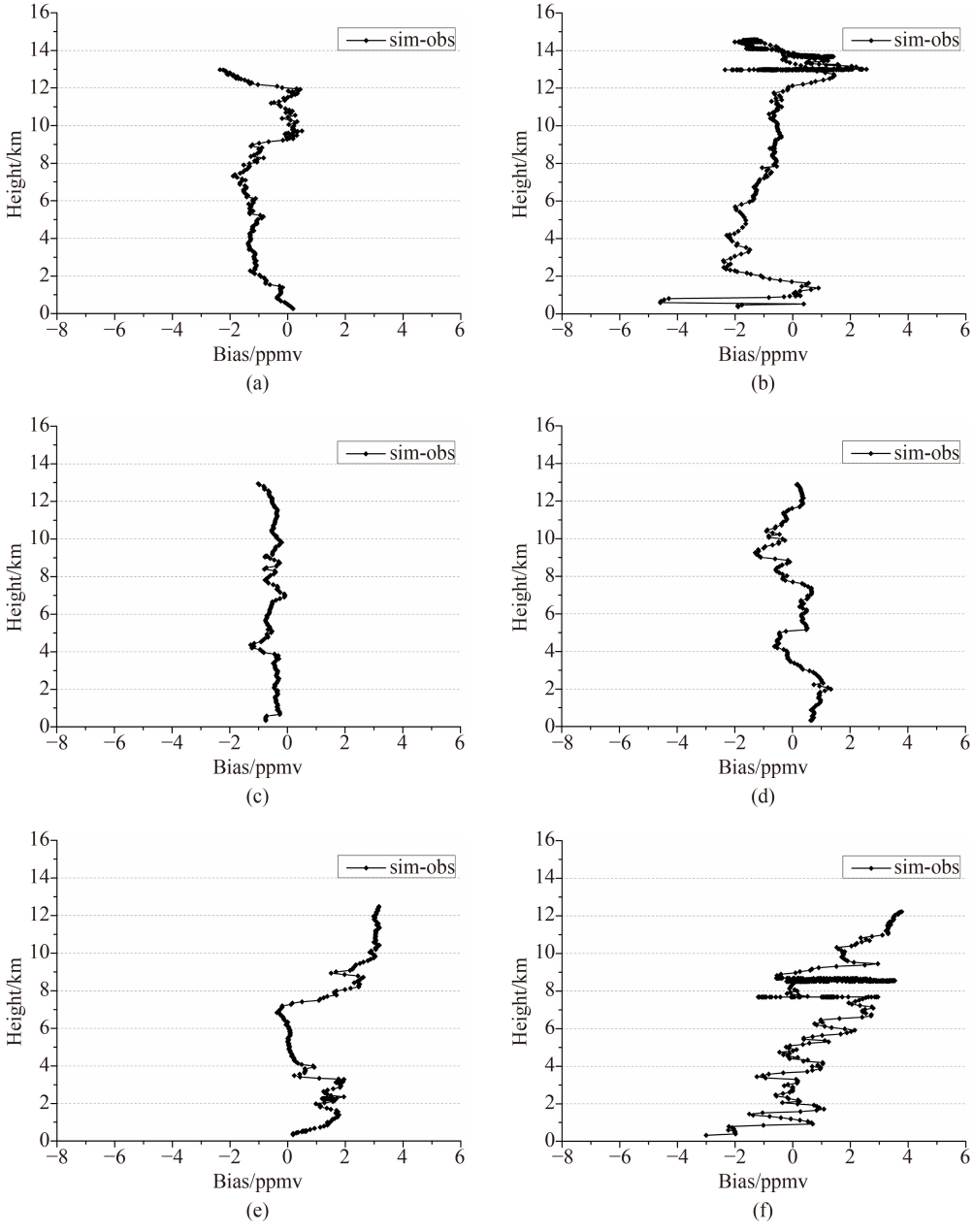

Fig. 5 Biases of simulation minus observation from near surface to the LS for HIPPO-1, Figures are corresponding to Figs. 4(a)–4(f), respectively.

Figure 6(b) also shows this phenomenon above 10 km. In the low latitudes (Fig. 6(c) and (d)), the simulations match well with observations. From near surface to the UT, the potential temperature gradient is smooth and biases are less than 1 ppmv, which indicates good performance. For the middle latitudes of the northern hemisphere, Fig. 6(e) shows relatively good simulation performance. However, as shown in Fig. 6(f), high latitudes did not perform well in the near surface or the middle and low troposphere. Compared with observations, the simulation profiles do not appear to reflect the original shape. Moreover, Fig. 7 further displays the biases of simulation minus observation corresponding to Figs. 6(a)–6(f), respectively.

As shown by HIPPO-3 data, the biases increase abruptly with flight height for the middle to high latitudes of the northern hemisphere with values reaching 7 ppmv. In the high latitudes of the southern hemisphere (Fig. 8(a)), the simulation underestimates the observations, and the absolute biases from the near surface to the LS are isostatic, less than 3 ppmv. The southern hemisphere low latitudes (Fig. 8(c)) indicate good performance of the simulations, where all biases are less than 1 ppmv. In the northern hemisphere low latitudes (Fig. 8(d)), the entire simulation appears to match well with observations. However, some locations do not reproduce the precise

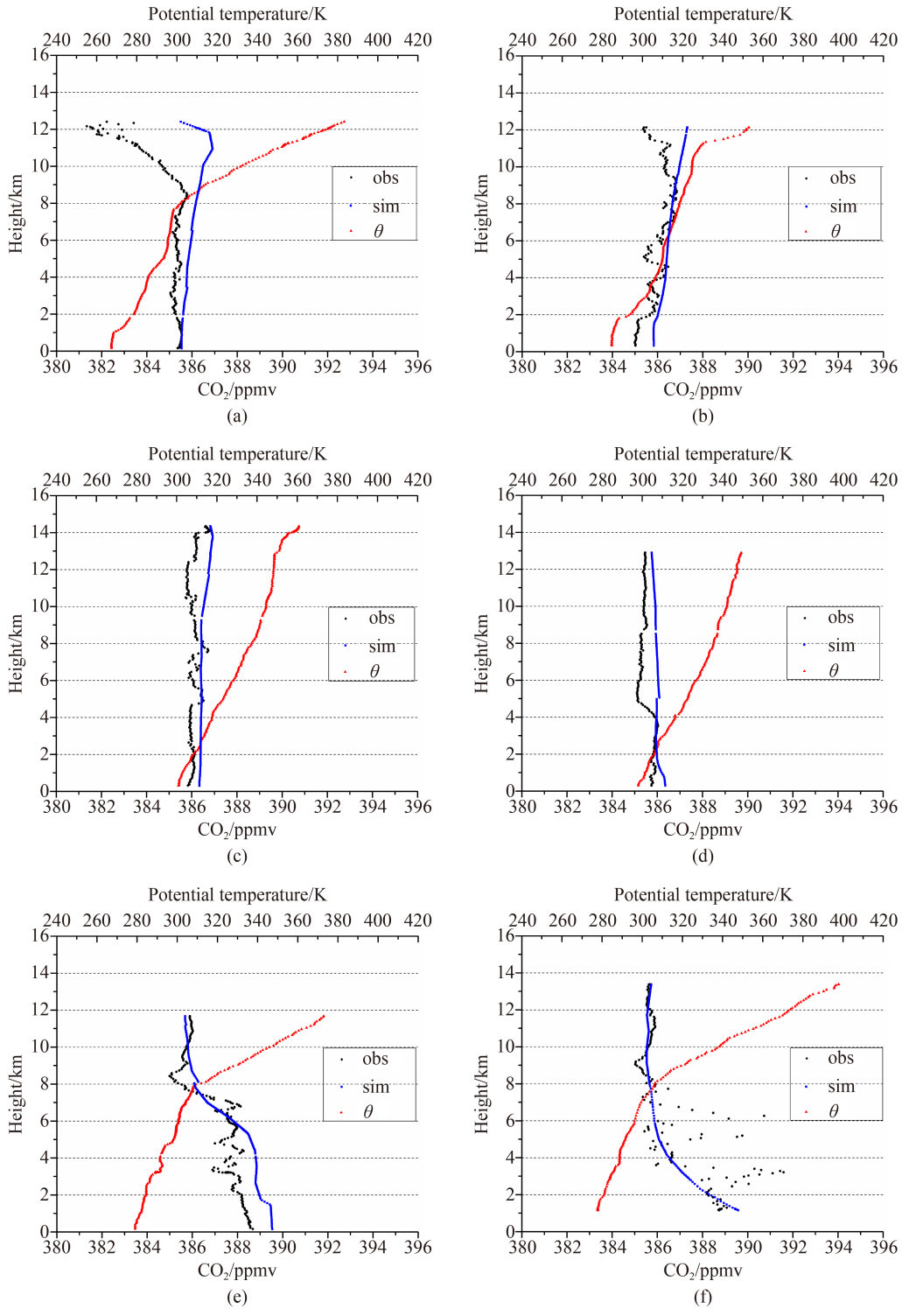

Fig. 6 Vertical profiles from near surface to the LS for HIPPO-2, Figures represent the vertical profiles of observation (black square), simulation (blue square) and potential temperature (red square) in southern ((a) high, (b) middle, (c) low latitude), and northern hemisphere ((d) low, (e) middle, (f) high latitude).

shape through the entire height. For the middle to high northern latitudes (Figs. 8(e) and 8(f)), the simulations performed relatively well from the near surface to the UT. Furthermore, Fig. 9 shows the biases of simulation minus observation corresponding to Figs. 8(a)–8(f), respectively.

A large bias is found in simulations of the lower stratosphere in winter in the northern high latitudes. The reason for this problem is that between the tropopause and 350 K level, the model uses vertical wind provided by reanalysis rather than a more accurate radiative

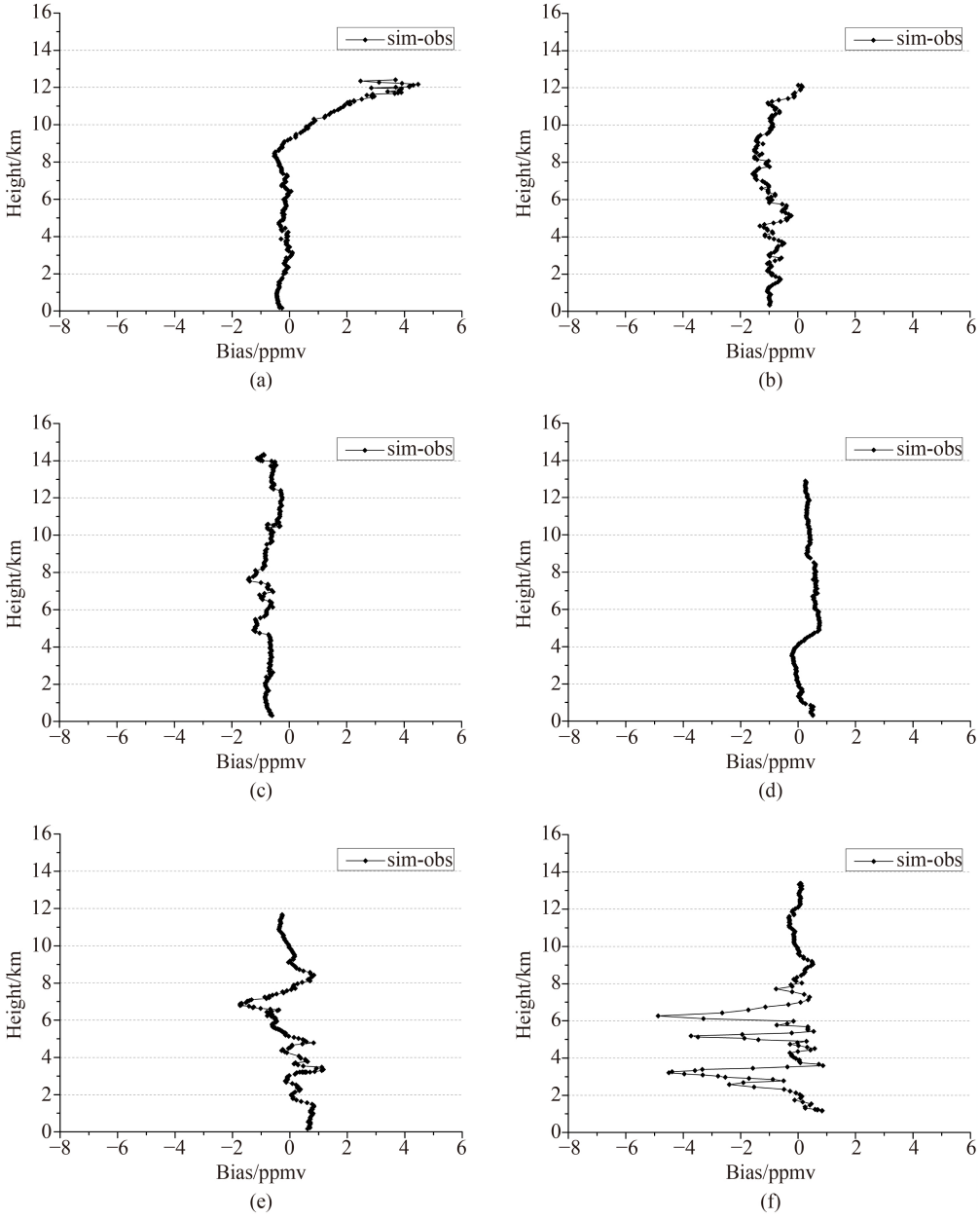

Fig. 7 Biases of simulation minus observation from near surface to the LS for HIPPO-2, figures are corresponding to Figs. 6(a)–6(f), respectively.

heating rate in the stratosphere (Weaver et al., 1993, Belikov et al., 2013). Extending isentropic coordinates to the middle troposphere, such as the method implemented by Chen and Rasch (2012), Bleck et al. (2015), has the potential to reduce the transport bias in this region and season. The positive bias of CO_2 can reach 4 ppmv. However, when the tropopause level is low, this problem only affects simulations for observation made in the lower stratosphere in high latitudes in cold season. However, the number of in situ observations made at this height is very limited. The satellite observations of total column such as GOSAT are also reduced considerably in high latitudes in cold season (Yoshida et al., 2013). Thus, this lower stratosphere bias is unlikely to deteriorate the transport model performance in inverse modeling applications (Maksyutov et al., 2013). However, these biased values probably result in greater errors of a flux inversion with signals being transported into lower latitudes in adverse synoptic patterns.

4 Conclusions

This study tested and verified the capability of a chemistry transport model that reproduces CO_2 vertical profiles of missions 1 to 3 using HIPPO merged 10-s meteorology, atmospheric chemistry, and aerosol data.

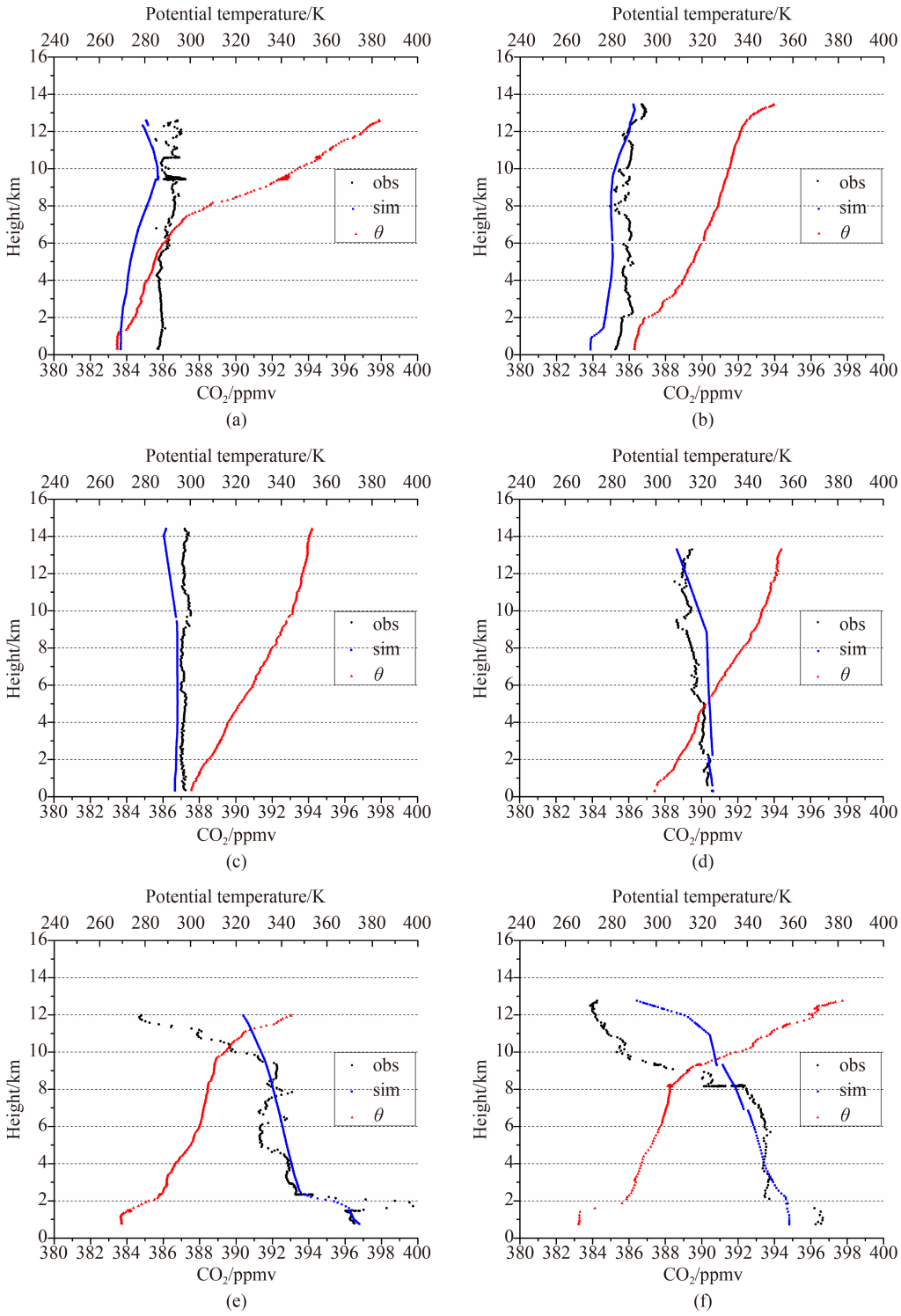

Fig. 8 Vertical profiles from near surface to the LS for HIPPO-3, figures represent the vertical profiles of observation (black square), simulation (blue square) and potential temperature (red square) in southern ((a) high, (b) middle, (c) low latitude), and northern hemispheres ((d) low, (e) middle, (f) high latitude).

Missions 1 to 3 span three different seasons (autumn, winter and spring).

The results were analyzed for diurnal variations and compared with observed CO_2 in January and November, 2009, and March and April, 2010. The validation results demonstrate the simulation precision and good performance of the model compared with observed CO_2. The resulting low biases between observed and simulated for HIPPO-1 time-varying CO_2 concentrations are highly promising (approximately 69.2% within 1 ppmv, ~92.3%

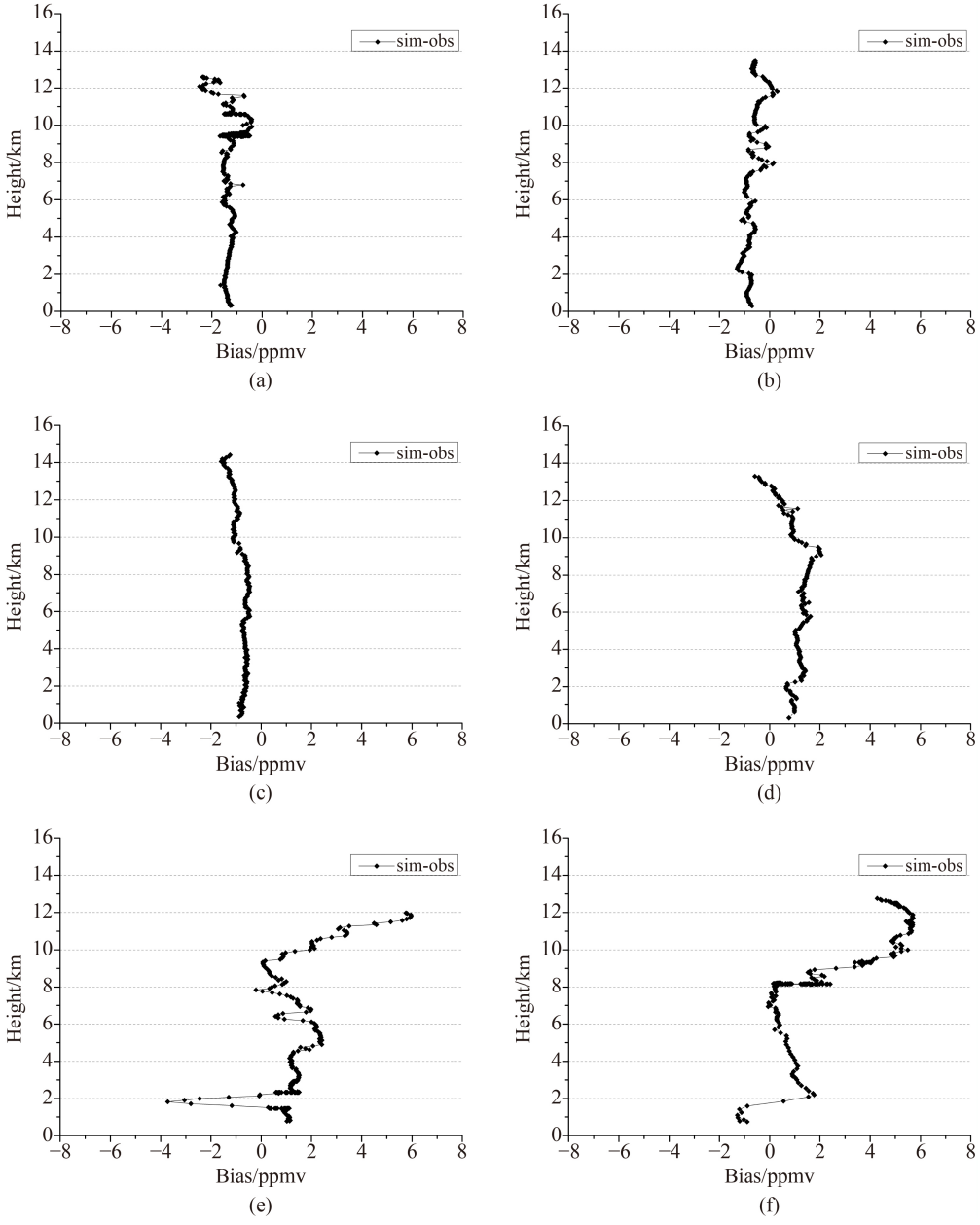

Fig. 9 Biases of simulation minus observation from near surface to the LS for HIPPO-3, figures are corresponding to Figs. 8(a)–8(f), respectively.

within 2 ppmv, and ~7.7% within 3 ppmv) and RMSE are stable for most days during the study period. The analytical results indicate, using the same observed and simulated CO_2 concentration latitude-varying data, that atmospheric XCO_2 is always underestimated and differences are all within 1.5 ppmv in the southern hemisphere, and vice versa in the northern hemisphere with 85.8% of the differences under 1.1 ppmv, and the mutable values reflect the instability of the simulated values at northern hemisphere high latitudes. The statistical analysis of the HIPPO-2 and 3 simulated missions are similar to the findings of the HIPPO-1 analysis.

The results show that the model somewhat underestimates CO_2 in the southern hemisphere and overestimates in the northern hemisphere for these three missions. However, the model was able to reproduce the seasonal and inter-annual variability of CO_2 with RMS bias across all profiles with a level of 0.9 ppmv. The model performed well from the near surface to the top of the troposphere, except for the lower stratosphere in high latitudes, especially in the northern hemisphere in spring, where large biases often appear. The smaller bias for HIPPO-1 compared with HIPPO-3 arises from seasonal changes in synoptic patterns from January to March and

April, as simulated by Patra et al. (2008).

The accuracy of these calculations will increase with the adaptation of the mass-balanced reanalysis data (MERRA; Bosilovich et al., 2008). This off-line model with horizontal flux-correction attains mass conservation, because vertically integrated mass change is in balance with surface pressure tendency (Belikov et al., 2011). The computation achieves rapid convergence, and the CO_2 distribution tends to be stable in the whole integral height. The demand for global high-resolution CO_2 and other greenhouse gases fields will also increase, as they are used as a priori information in retrieval algorithms of observation instruments, such as the AIRS satellite (e.g., Strow and Hannon, 2008) and GOSAT (e.g., Yokota et al., 2009), and regional inverse modeling studies (Thompson et al., 2014). The NIES model is verified by HIPPO-1, 2, 3, which provides basis for the applying high-precision satellite products, so as to obtain more and better carbon sources/sinks information.

Acknowledgments The authors acknowledge NSF, EOL of NCAR and NOAA which supported the collection of the original HIPPO data. This project was supported by the National Basic Research Program of China (No. 2010CB951603). The computation was supported by the High Performance Computer Center of East China Normal University. We thank the team members of the Biogeochemical Cycle Modeling and Analysis Section of National Institute for Environment Studies, Tsukuba, Japan for providing expert advice and assistance. The GOSAT Level 4 data made available by GOSAT project.

References

Baker D F, Law R M, Gurney K R, Rayner P, Peylin P, Denning A S, Bousquet P, Bruhwiler L, Chen Y H, Ciais P, Fung I Y, Heimann M, John J, Maki T, Maksyutov S, Masarie K, Prather M, Pak B, Taguchi S, Zhu Z (2006). TransCom 3 inversion intercomparison: impact of transport model errors on the interannual variability of regional CO_2 fluxes 1988–2003. Global Biogeochem Cy, 20: GB1002

Belikov D, Maksyutov S, Miyasaka T, Saeki T, Zhuravlev R, Kiryushov B (2011). Mass-conserving tracer transport modeling on a reduced latitude-longitude grid with NIES-TM. Geosci Model Dev, 4(1): 207–222

Belikov D, Maksyutov S, Sherlock V, Aoki S, Deutscher N M, Dohe S, Griffith D, Kyro E, Morino I, Nakazawa T, Notholt J, Rettinger M, Schneider M, Sussmann R, Toon G C, Wennberg P O, Wunch D (2013). Simulations of column-averaged CO_2 and CH_4 using the NIES TM with a hybrid sigma-isentropic (σ-θ) vertical coordinate. Atmos Chem Phys, 13(4): 1713–1732

Belikov D, Sugawara S, Ishidoya S, Hasebe F, Maksyutov S, Aoki S, Morimoto S, Nakazawa T (2019). Three-dimensional simulation of stratospheric gravitational separation using NIES global atmospheric tracer transport model. Atmos Chem Phys, 19(8): 5349–5361

Bleck R, Bao J W G, Benjamin S, Brown J M, Fiorino M, Henderson T B, Lee J L, MacDonald A E, Madden P, Middlecoff J, Rosinski J, Smirnova T G, Sun S, and N Wang (2015). A vertically flow-following icosahedral grid model for medium-range and seasonal prediction. Part I: model description. Mon Wea Rev, 143: 2386–2403.

Bolin B, Keeling C D (1963). Large-scale atmospheric mixing as deduced from seasonal and meridional variations of the atmospheric carbon dioxide. J Geophys Res, 68(13): 3899–3920

Bosilovich M G, Chen J, Robertson F R, and Adler R F (2008). Evaluation of global precipitation in reanalysis. J Appl Meteor Climatol, 47: 2279–2299

Bregman B, Meijer E, Scheele R (2006). Key aspects of stratospheric tracer modeling using assimilated winds. Atmos Chem Phys, 6(12): 4529–4543

Chen C C, Rasch P J (2012). Climate Simulations with an Isentropic Finite-Volume Dynamical Core. J Clim, 25(8): 2843–2861

Dee D P, Uppala S (2009). Variational bias correction of satellite radiance data in the ERA-Interim reanalysis. Q J R Meteorol Soc, 135(644): 1830–1841

Denning A S, Randall D A, Collatz G J, Sellers P J (1996). Simulations of terrestrial carbon metabolism and atmospheric CO_2 in a general circulation model. Part II: simulated CO_2 concentrations. Tellus B Chem Phys Meterol, 48(4): 543–567

Denning A S, Holzer M, Gurney K R, Heimann M, Law R M, Rayner P J, Fung I Y, Fan S M, Taguchi S, Friedlingstein P, Balkanski Y, Taylor J, Maiss M, Levin I (1999). Three-dimensional transport and concentration of SF6: a model intercomparison study (TransCom2). Tellus B Chem Phys Meterol, 51(2): 266–297

Douglass A R, Prather M J, Hall T M, Strahan S E, Rasch P J, Sparling L C, Coy L, Rodriguez J M (1999). Choosing meteorological input for the global modeling initiative assessment of high-speed aircraft. J Geophys Res, 104(D22): 27545–27564

GLOBALVIEW-CO_2 (2013). Cooperative Atmospheric Data Integration Project–Carbon Dioxide, CD-ROM, NOAA ESRL. Boulder: Colorado

Gurney K R, Law R M, Denning A S, Rayner P J, Pak B C, Baker D, Bousquet P, Bruhwiler L, Chen Y H, Ciais P, Fung I Y, Heimann M, John J, Maki T, Maksyutov S, Peylin P, Prather M, and Taguchi, S (2004). Transcom 3 inversion intercomparison: model mean results for the estimation of seasonal carbon sources and sinks. Global Biogeochem Cy, 18: GB1010

Hack J J, Boville B A, Briegleb B P, Kiehl J T, Rasch P J, Williamson D L (1993). Description of the NCAR community climate model (CCM2). Ncar Technical Note

Hall T M, Waugh D W, Boering K A, Plumb R A (1999). Evaluation of transport in stratospheric models. J Geophys Res, 104(D15): 18815–18839

Hein R, Crutzen P J, Heimann M (1997). An inverse modeling approach to investigate the global atmospheric methane cycle. Global Biogeochem Cycles, 11(1): 43–76

IPCC (2016) Intergovernmental Panel on Climate Change. Available at IPPC website

Jacob D, Prather M J, Rasch P J, Shia R L, Balkanski Y J, Beagley S R, Bergmann D J, Blackshear W T, Brown M, Chiba M, Chipperfield M P, de Grandpr'e J, Dignon J E, Feichter J, Genthon C, Grose W L, Kasibhatla P S, Köhler I, Kritz M A, Law K, Penner J E,

Ramonet M, Reeves C E, Rotman D A, Stockwell D Z, Van Velthoven P F J, Verver G, Wild O, Yang H, Zimmermann P (1997). Evaluation and intercomparison of global transport models using ^{222}Rn and other short-lived tracers. J Geophys Res, 102(D5): 5953–5970

Jöckel P, von Kuhlmann R, Lawrence M G, Steil B, Brenninkmeijer C A M, Crutzen P J, Rasch P J, Eaton B (2001). On a fundamental problem in implementing flux-form advection schemes for tracer transport in 3-dimensional general circulation and chemistry transport models. Q J R Meteorol Soc, 127(573): 1035–1052

Keppel-Aleks G, Wennberg P O, Schneider T (2010). Sources of variations in total column carbon dioxide. Atmos Chem Phys, 10: 30569–30611

Law R M, Peters W, Rödenbeck C, Aulagnier C, Baker I, Bergmann D J, Bousquet P, Brandt J, Bruhwiler, L, Cameron-Smith P J, Christensen J H, Delage F, Denning A S, Fan S M, Geels C, Houweling S, Imasu R, Karstens U, Kawa S R, Kleist J, Krol M, Lin S J, Lokupitiya R, Maki T, Maksyutov S, Niwa Y, Onishi R, Parazoo N, Patra P K, Pieterse G, Rivier L, Satoh M, Serrar S, Taguchi S, Takigawa M, Vautard R, Vermeulen A T, and Zhu Z (2008). Trans Commodel simulations of hourly atmospheric CO_2: experimental overview and diurnal cycle results for 2002. Global Biogeochem Cy, 22: GB3009

Mahowald N M, Plumb R A, Rasch P J, del Corral J, Sassi F (2002). Stratospheric transport in a three-dimensional isentropic coordinate model. J Geophys Res, 107(D15): 4254

Maksyutov S, Patra P K, Onishi R, Saeki T, Nakazawa T (2008). NIES/FRCGC global atmospheric tracer transport model: description, validation, and surface sources and sinks inversion. J Earth Simul, 9: 3–18

Maksyutov S, Takagi H, Valsala V K, Saito M, Oda T, Saeki T, Belikov D A, Saito R, Ito A, Yoshida Y, Morino L, Uchino O, Andres R J, Yokota T (2013). Regional CO_2 flux estimates for 2009–2010 based on GOSAT and ground-based CO_2 observations. Atmos Chem Phys, 13(18): 9351–9373

Maksyutov S, Oda T, Saito M, Janardanan R, Belikov D, Kaiser J W, Zhuravlev R, Ganshin A, Valsala V K, Andrews A, Chmura L, Dlugokencky E, Haszpra L, Langenfelds R L, Machida T, Nakazawa T, Ramonet M, Sweeney C, Worthy D (2021). Technicla note: A high-resolution inverse modelling technique for estimating surface CO_2 fluxes based on the NIES-TM-FLEXPAPT coupled transport model and its adjoint. Atmos Chem Phys, 21(2): 1245–1266

Monge-Sanz B M, Chipperfield M P, Simmons A J, Uppala S M (2007). Mean age of air and transport in a CTM: comparison of different ECMWF analyses. Geophys Res Lett, 34(4): L04801

Niwa Y, Patra P K, Sawa Y, Machida T, Matsueda H, Belikov D, Maki T, Ikegami M, Imasu R, Maksyutov S, Oda T, Satoh M, Takigawa M (2011). Three-dimensional variations of atmospheric CO_2: aircraft measurements and multi transport model simulations. Atmos Chem Phys, 11(24): 13359–13375

Onogi K, Tsutsui J, Koide H, Sakamoto M, Kobayashi S, Hatsushika H, Matsumoto T, Yamazaki N, Kamahori H, Takahashi K, Kadokura S, Wada K, Kato K, Oyama R, Ose T, Mannoji N, Taira R (2007). The JRA-25 reanalysis. J Meteorol Soc Jpn, 85(3): 369–432

Parker R, Boesch H, Cogan A, Fraser A, Feng L, Palmer P I, Messerschmidt J, Deutscher N, Griffith D W T, Notholt J, Wennberg P O, Wunch D (2011). Methane observations from the Greenhouse Gases Observing SATellite: comparison to ground based TCCON data and model calculations. Geophys Res Lett, 38(15): L15807

Patra P K, Maksyutov S, and Transcom-3 modelers (2003a). Sensitivity of optimal extension of observation networks to model transport. Tellus, 55(2): 498–511

Patra P K, Maksyutov S, Sasano Y, Nakajima H, Inoue G, and Nakazawa T (2003b). An evaluation of CO_2 observations with Solar Occultation FTS for Inclined-Orbit Satellite sensor for surface source inversion. J Geophys Res, 108(D24): 4759

Patra P K, Peters W, Rödenbeck C, Aulagnier C, Baker I, Bergmann D J, Bousquet P, Brandt J, Bruhwiler, L, Cameron-Smith P J, Christensen J H, Delage F, Denning A S, Fan S M, Geels C, Houweling S, Imasu R, Karstens U, Kawa S R, Kleist J, Krol M, Law R M, Lin S J, Lokupitiya R, Maki T, Maksyutov S, Niwa Y, Onishi R, Parazoo N, Pieterse G, Rivier L, Satoh M, Serrar S, Taguchi S, Takigawa M, Vautard R, Vermeulen A T, and Zhu Z (2008). TransCom model simulations of hourly atmospheric CO_2: analysis of synoptic-scale variations for the period 2002–2003. Global Biogeochem Cy, 22: GB4013

Patra P K, Houweling S, Krol M, Bousquet P, Belikov D, Bergmann D, Bian H, Cameron-Smith P, Chipperfield M P, Corbin K, Fortems-Cheiney A, Fraser A, Gloor E, Hess P, Ito, A, Kawa S R, Law R M, Loh Z, Maksyutov S, Meng L, Palmer P I, Prinn R G, Rigby M, Saito R, Wilson C (2011). Transcom model simulations of CH_4 and related species: linking transport, surface flux and chemical loss with CH_4 variability in the troposphere and lower stratosphere. Atmos Chem Phys, 11: 12813–12837

Rasch P J, Boville B A, Brasseur G P (1995). A three dimensional general circulation model with coupled chemistry for the middle atmosphere. J Geophys Res, 100(D5): 9041–9071

Raupach M R, Marland G, Ciais P, Le Quéré C, Canadell J G, Klepper G, Field C B (2007). Global and regional drivers of accelerating CO_2 emissions. Proc Natl Acad Sci USA, 104(24): 10288–10293

Rayner P J, Enting I G, Francey R J, Langenfelds R (1999). Reconstructing the recent carbon cycle from atmospheric CO_2, $\delta^{13}C$ and O_2/N_2 observations. Tellus B Chem Phys Meterol, 51(2): 213–232

Rayner P J, O'Brien D M (2001). The utility of remotely sensed CO_2 concentration data in surface inversion. Geophys Res Lett, 28(1): 175–178

Scholes R J, Monteiro P M S, Sabine C L, Canadell J G (2009). Systematic long-term observations of the global carbon cycle. Trends Ecol Evol, 24(8): 427–430

Schoeberl M R, Douglass A R, Zhu Z, Pawson S (2003). Acomparison of the lower stratospheric age spectra derived from a general circulation model and two data assimilation systems. J Geophys Res, 108(D3): 4113

Stohl A, Cooper O, James P (2004). A cautionary note on the use of meteorological analysis data for quantifying atmospheric mixing. J Atmos Sci, 61(12): 1446–1453

Strow L L, Hannon S E (2008). A 4-year zonal climatology of lower tropospheric CO_2 derived from ocean-only Atmospheric Infrared Sounder observations. J Geophys Res, 113(D18): D18302

Tans P P, Fung I Y, Takahashi T (1990). Observational contrains on the global atmospheric CO_2 budget. Science, 247(4949): 1431–1438

Thompson R L, Ishijima K, Saikawa E, Corazza M, Karstens U, Patra P K, Bergamaschi P, Chevallier F, Dlugokencky E, Prinn R G, Weiss R F, O'Doherty S, Fraser P J, Steele L P, Krummel P B, Vermeulen A, Tohjima Y, Jordan A, Haszpra L, Steinbacher M, Van der Laan S, Aalto T, Meinhardt F, Popa M E, Moncrieff J, Bousquet P (2014). TransCom N_2O model inter-comparison–Part 2: atmospheric inversion estimates of N_2O emissions. Atmos Chem Phys, 14(12): 6177–6194

Waugh D W, Hall T M (2002). Age of stratospheric air: theory, observations, and models. Rev Geophys, 40(4): 1010

Weaver C J, Douglass A R, Rood R B (1993). Thermodynamic balance of three-dimensional stratospheric winds derived from a data assimilation procedure. J Atmos Sci, 50(17): 2987–2993

Wofsy S C, Daube B C, Jimenez R, Kort E, Pittman J V, Park S, Commane R, Xiang B, Santoni G, Jacob D, Fisher J, Pickett-Heaps C, Wang H, Wecht K, Wang Q Q, Stephens B B, Shertz S, Watt A S, Romashkin P, Campos T, Haggerty J, Cooper W A, Rogers D, Beaton S, Hendershot R, Elkins J W, Fahey D W, Gao R S, Moore F, Montzka S A, Schwarz J P, Perring A E, Hurs D, Miller B R, Sweeney C, Oltmans S, Nance D, Hintsa E, Dutton G, Watts L A, Spackman J R, Rosenlof K H, Ray E A, Hall B, Zondlo M A, Diao M, Keeling R, Bent J, Atlas E L, Lueb R, Mahoney M J (2012). HIPPO Merged 10-second Meteorology, Atmospheric Chemistry. Aerosol Data (R_20121129) Carbon Dioxide Information Analysis Center, Oak Ridge National Laboratory, Oak Ridge, Tennessee, USA

Wunch D, Toon G, Blavier J F L, Washenfelder R A, Notholt J, Connor B J, Griffith D W T, Sherlock V, Wennberg P O (2011). The total carbon column observing network. Philos Trans Royal Soc, Math Phys Eng Sci A, 369(1943): 2087−2112

Yang Z, Washenfelder R A, Keppel-Aleks G, Krakauer N Y, Randerson J T, Tans P P, Sweeney C, Wennberg P O (2007). New constraints on Northern Hemisphere growing season net flux. Geophys Res Lett, 34(12): L12807

Yokota T, Yoshida Y, Eguchi N, Ota Y, Tanaka T, Watanabe H, Maksyutov S (2009). Global concentrations of CO_2 and CH_4retrieved from GOSAT: first preliminary results. Sci Online Lett Atmos, 5: 160–163

Yoshida Y, Kikuchi N, Morino I, Uchino O, Oshchepkov S, Bril A, Saeki T, Schutgens N, Toon G C, Wunch D, Roehl C M, Wennberg P O, Griffith D W T, Deutscher N M, Warneke T, Notholt J, Robinson J, Sherlock V, Connor B, Rettinger M, Sussmann R, Ahonen P, Heikkinen P, Kyrö E, Mendonca J, Strong K, Hase F, Dohe S, Yokota T (2013). Improvement of the retrieval algorithm for GOSAT SWIR XCO_2 and XCH_4 and their validation using TCCON data. Atmos Meas Tech, 6(6): 1533–1547

AUTHOR BIOGRAPHIES

Ci SONG is a lecturer of College of Science, Zhongyuan University of Technology, she was a post-doctor of School of Communication and Information Engineering, Shanghai University from 2018 to 2021. She received her B.S. in mathematics and applied mathematics from Henan Normal University in 2008, M.S. in mathematics and applied mathematics from East China Normal University and Ph.D. in physical geography from East China Normal University. Her research interests include remote sensing information processing and application, remote sensing mechanism and radiation transmission.

Shamil MAKSYUTOV is a researcher at Center for Global Environmental Research, National Institute for Environmental Studies, Tsukuba, Japan. He was a sub-leader at Japan Agency for Marine-Earth Science Technology from 2002 to 2005, a visiting researcher at National Institute for Environmental Studies from 1990 to 2000, a researcher at Department of Kinetics and Catalysis, Semenov Institute of Chemical Physics, Moscow, Russia. He had been studying in Moscow Institute of Physics and Technology from 1974 to 1983. His research interests include GHG observations and analysis and CO_2 transport modeling.

Jiong SHU is currently a professor of climatology at the Key Laboratory of Geographic Information Science, East China Normal University. He was an Honor Research Fellow at the University of Liverpool, UK, in 1999, after which he was employed as a Professor at the College of Resources and Environmental Science, East China Normal University in 2000. He joined the Key Laboratory of Geographical Information Science, Ministry of Education, in 2002 as the director until December 2009. His research interests include climate change and environmental remote sensing.